JCI The Journal of Clinical Investigation

ALK-transformed mature T lymphocytes restore early thymus progenitor features

Annabelle Congras, … , Laurence Lamant, Fabienne Meggetto

J Clin Invest. 2020;130(12):6395-6408. https://doi.org/10.1172/JCI134990.

Research Article Hematology

Graphical abstract

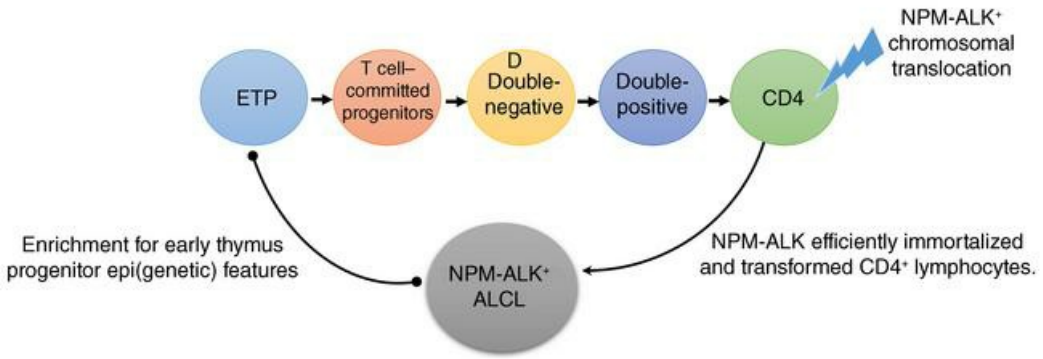

ALK-transformed mature T lymphocytes restore early thymus progenitor features

Annabelle Congras,[1,2,3,4] Coralie Hoareau-Aveilla,[1,2,3,4] Nina Caillet,[1,2,3,4] Marie Tosolini,[1,2,3,5] Patrick Villarese,[6] Agata Cieslak,[6] Laura Rodriguez,[7] Vahid Asnafi,[6] Elisabeth Macintyre,[6] Gerda Egger,[8,9] Pierre Brousset,[1,2,3,4,10,11] Laurence Lamant,[1,2,3,4,10,11,12] and Fabienne Meggetto[1,2,3,4,6,10,11,12]

[1]INSERM, UMR1037 CRCT, F-31000, Toulouse, France. [2]Université Toulouse III-Paul Sabatier, UMR1037 CRCT, F-31000, Toulouse, France. [3]CNRS, ERL5294 UMR1037 CRCT, F-31000, Toulouse, France. [4]Equipe Labellisée LIGUE 2017, Toulouse, France. [5]Pôle Technologique du CRCT, Plateau Bioinformatique, Toulouse, France. [6]Hematology and INSERM1151, Institut Necker-Enfants Malades, University Sorbonne Paris Cité at Descartes and Assistance Publique-Hopitaux de Paris, Paris, France. [7]Etablissement Français du Sang, Nouvelle Aquitaine, INSERM U1035, Université de Bordeaux, Bordeaux, France. [8]Department of Pathology, Medical University Vienna, Vienna, Austria. [9]Ludwig Boltzmann Institute Applied Diagnostics, Vienna, Austria. [10]Institut Carnot Lymphome, Toulouse, France. [11]Laboratoire d'Excellence Toulouse Cancer and after Cancer (Labex TOUCAN), Toulouse, France. [12]European Research Initiative on ALK-Related Malignancies, Cambridge, United Kingdom, Vienna, Austria, and Toulouse, France.

Anaplastic large cell lymphoma (ALCL) is a mature T cell neoplasm that often expresses the CD4$^+$ T cell surface marker. It usually harbors the t(2;5) (p23;q35) translocation, leading to the ectopic expression of NPM-ALK, a chimeric tyrosine kinase. We demonstrated that in vitro transduction of normal human CD4$^+$ T lymphocytes with NPM-ALK results in their immortalization and malignant transformation. The tumor cells displayed morphological and immunophenotypical characteristics of primary patient–derived anaplastic large cell lymphomas. Cell growth, proliferation, and survival were strictly dependent on NPM-ALK activity and include activation of the key factors STAT3 and DNMT1 and expression of CD30 (the hallmark of anaplastic large-cell lymphoma). Implantation of NPM-ALK–transformed CD4$^+$ T lymphocytes into immunodeficient mice resulted in the formation of tumors indistinguishable from patients' anaplastic large cell lymphomas. Integration of "Omic" data revealed that NPM-ALK–transformed CD4$^+$ T lymphocytes and primary NPM-ALK$^+$ ALCL biopsies share similarities with early T cell precursors. Of note, these NPM-ALK$^+$ lymphoma cells overexpress stem cell regulators (*OCT4*, *SOX2*, and *NANOG*) and HIF2A, which is known to affect hematopoietic precursor differentiation and NPM-ALK$^+$ cell growth. Altogether, for the first time our findings suggest that NPM-ALK could restore progenitor-like features in mature CD30$^+$ peripheral CD4$^+$ T cells, in keeping with a thymic progenitor-like pattern.

Introduction

Systemic anaplastic large cell lymphomas (ALCLs) account for 2% to 8% of non–Hodgkin's lymphomas in adults and approximately 10% to 30% of lymphomas in children. The majority (80%) of systemic ALCLs contain a t(2;5) chromosomal translocation that fuses the 3′ part of the anaplastic lymphoma kinase (*ALK*) gene on chromosome 2p23, with the 5′ part of the nucleophosmin (*NPM1*) gene on chromosome 5q35 (1). This translocation leads to the ectopic expression of a chimeric tyrosine kinase, NPM-ALK, which is oncogenic and activates a number of signal transduction pathways, including those implicating the transcription factor STAT3 to promote cell proliferation and survival (2). Systemic NPM-ALK$^+$ ALCL frequently involves both lymph nodes and extranodal sites and is most common in children and young adults but can occur in older adults (3). This lymphoma shows a broad spectrum of morphological features from the common type (60%) characterized by large lymphoid cells often with horseshoe- or kidney-shaped nuclei to a small cell variant (4). It is considered a mature T cell lymphoma with an activated phenotype as all neoplastic cells display a constant expression of the CD30 molecule, a member of the tumor necrosis factor (TNF) receptor superfamily, normally expressed in activated lymphocytes (5). The vast majority of NPM-ALK$^+$ ALCLs express one or more T cell antigens. However, due to the loss of several pan–T cell antigens, some cases have a null T cell phenotype, but a clonally rearranged T cell receptor (TCR) β chain gene is detectable at the molecular level (50% to 60% of cases) even in tumor cells that do not express any obvious T cell–associated cell surface markers. CD3 and TCR expression are negative in more than 75% of cases. Surprisingly, CD4 expression is typically seen in a significant proportion of cases (>50%), whereas CD8 expression is rare (4, 6). NPM-ALK–activated STAT3 induces the expression of DNA methyltransferase 1 (DNMT1), the methylation of gene promoters epigenetically silencing several key genes from the TCR complex and its signalling pathway, including *CD3E*, *ZAP70*, *LAT*, and *SLP76*. This silencing contributes to the substantial loss of the T cell lineage identity seen in NPM-ALK$^+$ ALCL (7, 8). Epigenetic alterations, including DNA methylation, are key factors in stem cell differentiation (9). Recently, high throughput anal-

Authorship note: A Congras, CHA, and NC contributed equally.
Conflict of interest: The authors have declared that no conflict of interest exists.

Submitted: November 14, 2019; **Accepted:** August 11, 2020; **Published:** October 19, 2020.
Reference information: *J Clin Invest*. 2020;130(11):6395–6408.
https://doi.org/10.1172/JCI134990.

ysis of DNA methylation has been conducted on samples from patients with systemic NPM-ALK$^+$ ALCL in comparison with normal human T lymphocytes. It was reported that DNA methylation patterns in NPM-ALK$^+$ ALCL are related to specific thymic stages in T cell development, suggesting an early thymic progenitor CD34$^+$ CD1a$^-$ cell origin for NPM-ALK$^+$ ALCL (10, 11).

T cell development is initiated in the thymic subpopulation that lacks the cell surface expression of both CD4 and CD8 antigens. The earliest known T cell progenitors that seed the thymus are called early T cell progenitors (ETPs). Several transcription factors are critical for the emergence of ETPs, such as TCF7, LCK, GATA3, BCL11B, and LEF1, and are important for normal mature T cell development and function. Their expression is tightly regulated during normal T cell differentiation. Indeed, in thymic progenitors, they are repressed and hypermethylated but upon differentiation these genes are demethylated (12, 13). The fact that these 5 transcription factor genes are hypermethylated in NPM-ALK$^+$ ALCL suggests that this lymphoma originates from thymic progenitors (10). Moreover, it has been reported that NPM-ALK$^+$ ALCL cell lines and primary tumors are enriched in a subpopulation of cells with stem cell–like properties (11). Gene set enrichment analysis suggested that NPM-ALK$^+$ ALCL cell lines present an enriched gene expression profile associated with ETPs and express pluripotency-associated transcription factors, such as OCT4, SOX2, and NANOG, which can be activated by the transcriptional activator hypoxia inducible factor 2 (HIF2A) (11, 14). On the other hand, it has been reported that the NPM-ALK transgene could transform normal human CD4$^+$ peripheral mature T lymphocytes into ALCL cells from consecutive experiments of 3 separate pools of preactivated CD4$^+$ T cells (15). Thus, even though ALCL cells are believed to correspond to mature CD4$^+$ T lymphocytes, the origin of NPM-ALK$^+$ ALCL has not yet been convincingly demonstrated. It may be relevant in this context that the NPM-ALK fusion kinase is able to immortalize normal human CD4$^+$ T lymphocytes in vitro. To address this important question, we established in vitro models of NPM-ALK$^+$ ALCL by expressing NPM-ALK in normal CD4$^+$ T lymphocytes from 12 independent experiments, and conducted high throughput DNA methylation and transcriptomic analyses.

Results

NPM-ALK ectopic expression in normal CD4$^+$ T lymphocytes induces morphological and phenotypical changes reminiscent of ALK$^+$ anaplastic large cell lymphoma. In order to study the extent to which NPM-ALK is involved in reprogramming mature T cells into a thymic progenitor-like pattern, we ectopically expressed NPM-ALK in normal human mature T lymphocytes. We chose to use CD4$^+$ T lymphocytes, as approximately 50% of ALK$^+$ ALCLs are CD4$^+$. Peripheral blood mononuclear cells from healthy donors were used as starting material to isolate CD4$^+$ T lymphocytes. Lentiviral vectors encoding NPM-ALK were used to transduce these purified CD4$^+$ T lymphocytes that were preactivated with CD3 and CD28 antibodies to optimize an efficient transduction. Twelve independent experiments were conducted to produce 9 CD4$^+$ NPM-ALK$^+$ cell models designated CD4$^+$/NPM-ALK$^+$. In these 9 independent CD4$^+$/NPM-ALK$^+$ cell models, the expression of NPM-ALK, evaluated by real-time quantitative reverse transcription PCR (qRT-PCR) using NPM-ALK$^+$ ALCL cell lines KARPAS-299, COST, and SU-DHL-1 as positive controls, was confirmed (Figure 1A, CD4$^+$/NPM-ALK$^+$ lane shows the mean from the 9 independent models). In addition, similar to the NPM-ALK$^+$ ALCL–derived KARPAS-299 cell control, the CD4$^+$/NPM-ALK$^+$ cells displayed expression and phosphorylation of the NPM-ALK kinase and phosphorylation of STAT3, a well-characterized direct target of NPM-ALK (Figure 1B). Thus, we examined the effect of crizotinib, a pharmacological inhibitor of ALK, on NPM-ALK activity and cell proliferation in CD4$^+$/NPM-ALK$^+$ models. Crizotinib inhibited the catalytic activity of ALK, i.e. the phosphorylation of ALK, and as expected, there was a decrease in STAT3 activation (p-STAT3 protein levels) (Figure 1B). Moreover, proliferation of CD4$^+$/NPM-ALK$^+$ cells was significantly inhibited by crizotinib treatment or si-RNA directed against ALK mRNA (si-ALK) or STAT3 (si-STAT3) (Supplemental Figure 1, A and B; supplemental material available online with this article; https://doi.org/10.1172/JCI134990DS1). In order to check that the knockdown of gene expression had been efficiently achieved, we performed Western blotting to detect ALK and STAT3 protein levels (Supplemental Figure 1C). Finally, because the epigenetic silencing of genes in NPM-ALK$^+$ cells is due to the activation of STAT3 in cooperation with DNMT1 (Supplemental Figure 2A) (7, 8), we repressed the STAT3/DNMT1 axis using the small molecule inhibitor Stattic, or demethylating drugs such as 5-aza-2′-deoxycytidine/decitabine. As shown in Supplemental Figure 2B, both treatments induced an antiproliferative effect on NPM-ALK–transformed CD4$^+$ T lymphocytes. Taken together, these findings show that NPM-ALK–expressing CD4$^+$ T cells are addicted to the activation of the NPM-ALK/STAT3/DNMT1 axis for their growth.

We then examined the immunophenotype of NPM-ALK–expressing CD4$^+$ T cells. As observed by flow cytometry, CD4$^+$/NPM-ALK$^+$ cells, such as preactivated healthy CD4$^+$ T cells, showed a high CD30 expression and but associated with a pronounced loss of CD3 and TCRα/β (Figure 2 and Supplemental Figure 3B, staining in green or red and isotype control in blue). Of note, during the establishment of immortal CD4$^+$/NPM-ALK cell lines, we performed a time course analysis of CD3 expression and observed a decrease in CD3 expression concomitantly to NPM-ALK expression (Supplemental Figure 3A). In addition, CD4$^+$/NPM-ALK$^+$ cells mimicked NPM-ALK$^+$ ALCL primary cells by variably expressing the T cell markers CD2, CD5, and CD7 (Supplemental Table 1, mean from the 9 models). By contrast, NPM-ALK–expressing CD4$^+$ T cells were negative for CD8 and both B lymphocyte markers CD19 and CD20 (Supplemental Table 1, mean from the 9 models). To further characterize CD4$^+$/NPM-ALK$^+$ cells, we evaluated the variation in chromosome number (CNV) and clonality. As shown in Supplemental Figure 4, we did not highlight the changes relevant to the genome of NPM-ALK CD4$^+$ models. However, the TCR rearrangement PCR study indicated the monoclonal to oligoclonal nature of the CD4$^+$/NPM-ALK$^+$ cells (Supplemental Table 2). Furthermore, these CD4$^+$/NPM-ALK$^+$ cells were capable of forming tumors in vivo after subcutaneous xenotransplantation in immunodeficient NSG mice (Figure 3, A and B). These tumors were indistinguishable from NPM-ALK$^+$ ALCLs by their anaplastic large cell morphology: small- to medium-sized neoplastic cells with irregular nuclei; large hallmark cells always present; strong expression of NPM-ALK,

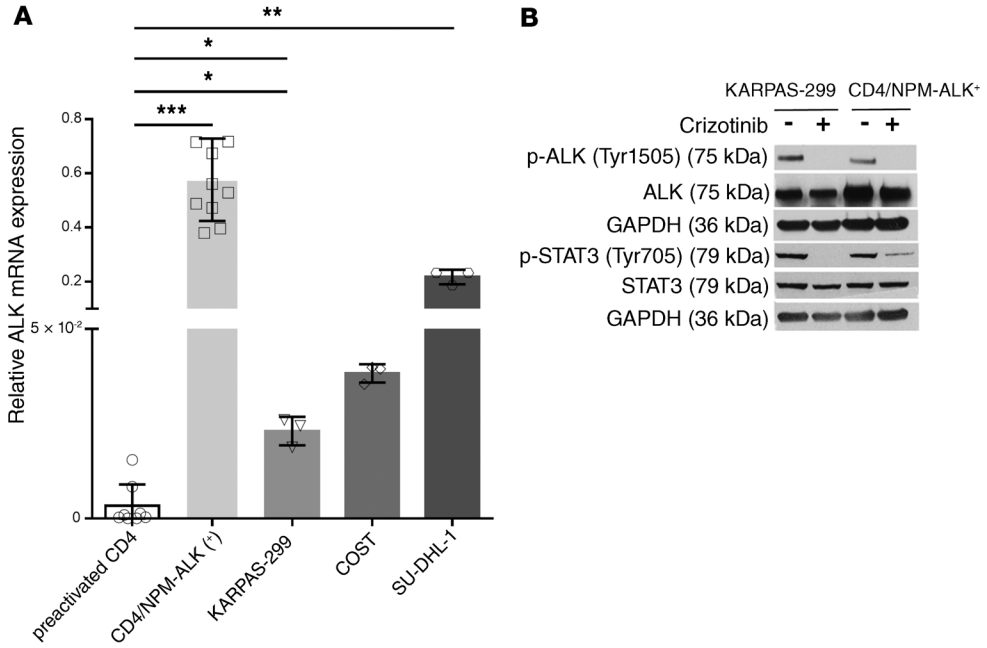

Figure 1. NPM-ALK dependence of the transformed CD4⁺ T cells. (**A**) Expression by qRT-PCR analysis of NPM-ALK mRNA in the transformed CD4⁺ T cells (CD4-NPM/ALK⁺ lane shows the mean from 9 independent cell lines) and 3 positive control NPM-ALK⁺ ALCL cell lines: KARPAS-299, SU-DHL-1, and COST. CD4⁺ T cells preactivated with CD3/CD28 antibody-coated beads were used as negative controls (preactivated CD4). MLNS1 was used as an internal control. Relative NPM-ALK expression was expressed as the 2–ΔCt relative to *MLN51*. Data represent mean ± SEM. $*P < 0.05$, $**P < 0.001$, $***P < 0.001$; unpaired 2-tailed Student's *t* test with Welch's correction. (**B**) Suppressive effect of the ALK inhibitor crizotinib (500 nmol/L) on ALK and STAT3 phosphorylation in transformed CD4⁺ T cells and control NPM-ALK⁺ KARPAS-299 cells. The GAPDH protein served as an internal control to ensure equal loading. Blots from 1 representative experiment are shown.

CD4, and CD30; and weak expression of the CD3 antigen (Figure 3C). To assess metastatic efficiency in vivo, we next injected either CD4⁺/NPM-ALK⁺ cells ($n = 7$) or PBS ($n = 3$) into the retroorbital veins of NSG mice. We assessed metastatic burden at 39 days. All mice presented with skin nodules without dermis and subcutis hyperplasia (Figure 4, A–C), and spleen hyperplasia (Figure 4D). A lymphomatous infiltration invaded the spleen and liver (Figure 4, E and F) and was also observed in skin lesions (Figure 4G). Some mice also displayed infiltration of malignant NPM-ALK⁺ cells in the gut and pancreas (Supplemental Figure 5, A and B). The neoplastic cells included a predominant population of small- to medium-sized neoplastic cells with irregular nuclei; large hallmark cells were always present. Many cells were fried-egg cells, i.e., cells with a pale cytoplasm and centrally located nuclei (Figures 4H, heads arrows), and ring-like nuclei could also be observed (Figure 4I, head arrows). Immunohistochemistry with the anti-ALK antibody performed on all tissue sections showed strong ALK staining in the large lymphoma cells as compared with the small variants (Figure 4, J and K). Small cells were often concentrated around blood vessels (Figure 4L). Of note, no significant involvement was found in the thymus (data not shown). In the last series of experiments, we determined the effects of NPM-ALK expression on tumor growth using crizotinib, and as shown in Supplemental Figure 6, A and B, crizotinib significantly impeded CD4⁺/NPM-ALK⁺ tumor cell growth in vivo. We then examined the effect of the drug on tumor cells using hematoxylin/eosin (H&E) staining in xenografted tumor tissues. As expected, H&E staining revealed that tumor necrotic areas were more extensive in tumors upon treatment with crizotinib (Supplemental Figure 6C, arrows) (16–19). Taken together, these data indicate that NPM-ALK efficiently immortalized and transformed CD4⁺ lymphocytes. NPM-ALK–transformed CD4⁺ cells are morphologically and immunophenotypically indistinguishable from the patient-derived ALK⁺ ALCL cells.

DNA methylation links NPM-ALK–transformed CD4⁺ cells and patient-derived NPM-ALK⁺ lymphoma cells to early thymic progenitor cells. As NPM-ALK–transformed CD4⁺ cells were indistinguishable from patient-derived NPM-ALK⁺ ALCL cells, we decided to compare the CD4⁺/NPM-ALK⁺ DNA methylome to NPM-ALK⁺ primary lymphoma cells. The Illumina Infinium HumanMethylation EPIC chip measures the DNA methylation of more than 850,000 CpG sites, including 99% of RefSeq genes and 95% of CpG islands, and was used to determine the DNA methylation status of NPM-ALK⁺ cells, i.e., NPM-ALK–transformed CD4⁺ cells and NPM-ALK⁺ primary ALCL cells. First, as several studies demonstrated that epigenetic age acceleration in blood was predictive of cancer (20, 21), and to show that NPM-ALK promotes cancer features, we analyzed the epigenetic acceleration of CD4⁺/NPM-ALK⁺ ($n = 9$) and healthy stimulated CD4⁺ lymphocytes ($n = 5$). As shown in Supplemental Figure 7A, we observed that NPM-ALK⁺ lymphoma cells exhibit significant epigenetic age acceleration compared with normal T lymphocytes. It is noteworthy that we also observed a significant difference in age acceleration between CD4⁺/NPM-ALK⁺ models compared with preactivated CD4⁺ matched controls ($n = 3$; Supplemental Figure 7B), suggesting that NPM-ALK promotes cancer features in human CD4⁺ lymphocytes. In a second step, in order to evaluate whether the DNA methylome of CD4⁺/NPM-ALK⁺ cells ($n = 9$) and NPM-ALK⁺ primary ALCL cells

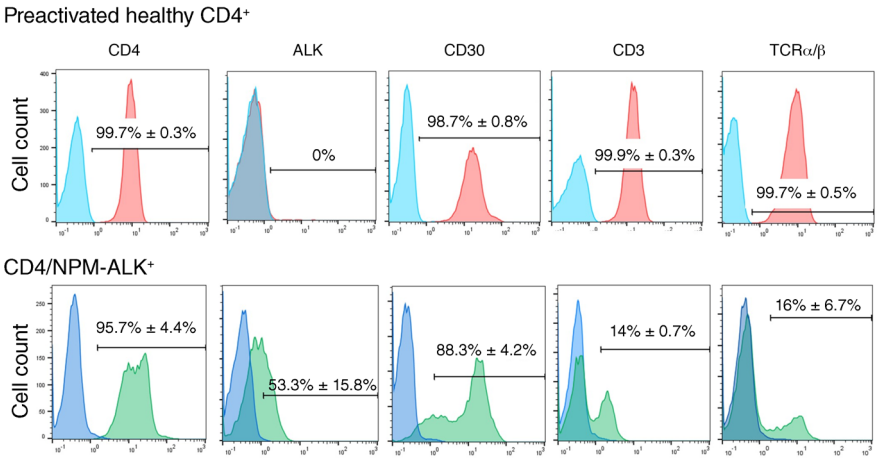

Figure 2. NPM-ALK–transformed CD4⁺ T lymphocytes immunophenotype. Normal CD4⁺ T cells prestimulated with CD3/CD28 antibody-coated beads were transduced with NPM-ALK and 40 days later flow cytometry analysis was performed to detect expression of T cell markers stained with an anti-ALK, -CD3, -CD4, -CD30, and -TCRαβ antibodies (NPM-ALK⁺ CD4⁺ T cells in green and prestimulated healthy CD4⁺ T cells in red) or IgG as control (blue). Preactivated human healthy CD4⁺ T cells were used as controls. Data are representative of the mean ± SEM from the 9 independent cell lines.

(n = 22) shared a close similarity with healthy T lymphocytes, we examined several cell populations isolated ex vivo from the neonatal human thymus, at various in vivo maturation stages. For this purpose, we integrated publicly available methylation data sets generated from different developmental T cell stages (22): multipotent ETPs (CD34⁺/CD1a⁻; n = 2), T cell–committed progenitors (CD34⁺/CD1a⁺; n = 1), pre-TCR T cells (n = 2), TCR-expressing CD4⁺/CD8⁺ double-positive T cells (DP-TCR⁺, n = 2), and single positive (SP) CD8⁺ or CD4⁺ cells (SP-CD4⁺; n = 2 or SP-CD8⁺; n = 2) (Figure 5A). We also incorporated the data from 5 NPM-ALK⁺ ALCL cases previously analyzed by Hassler et al. (10). All publicly available data were obtained using the Illumina Infinium HumanMethylation 450K BeadChip array.

First, in order to obtain a specific signature of DNA methylation during each step of human T cell differentiation, we decided to investigate a set of genomic regions spanning CpG sites that showed a specific methylation profile for each thymic developmental stage, i.e., ETPs, T cell–committed progenitors, DP-TCR⁺, SP-CD4⁺, and SP-CD8⁺. To identify such differentially methylated regions (DMRs), mean DNA methylation levels of multiple probes were calculated for distinct regions based on the annotated Illumina categories. DMRs with a nonadjusted P value less than 0.001 and in which at least 2 adjacent CpG sites had a minimum absolute DNA methylation difference of 0.3 were retained as significant. Despite the large scale of methylation changes, we identified a cluster of 510 DMRs that could be used to discriminate each stage of T cell differentiation in the thymus. The major fraction of the 510 DMRs was hypomethylated (n = 305; ~60%). When we assessed the relationship of DMRs to genes, we found that DMRs were associated with 238 genes and roughly 42% of DMRs were located in promoters (defined as up to 5 kb upstream from the start of the gene) (data not shown). Next, we found that roughly 24% of DMRs overlapped with DNase hypersensitive sites (Supplemental Figure 8A), suggesting overlap with regulatory DNA. Furthermore, over 70% of all DMRs also overlapped with known enhancer histone marks, H3K4me1 (72.5%) and H3K27me3 (77.8%) (Supplemental Figure 8A). These data suggest that DMRs overlap with regulatory DNA, most likely at enhancers, a pattern observed in other types of comparisons (23). Three hundred forty-five DMR-associated genes were significantly enriched with regard to T cell physiology (Supplemental Figure 8B). Finally, we measured the similarity of the 510 DMRs between the specific thymic stages in T cell development and NPM-ALK⁺ cells, i.e., CD4⁺/NPM-ALK⁺ cells (n = 9), and patient-derived NPM-ALK⁺ lymphoma cells (n = 27). We used Spearman rank correlation as a measure of pair-wise similarity of DMR profiles between samples. As shown in Figure 5B, we observed that both DMR profiles of NPM-ALK transformed CD4⁺ cells were distant to the healthy CD4⁺ lymphocyte profile and clustered with primary NPM-ALK⁺ ALCL cells. Heatmaps with the 510 DMRs at each differentiation step also showed a similarity of DMR profiles in ALK⁺ cells, i.e., NPM-ALK–transformed CD4⁺ cells and NPM-ALK⁺ lymphoma cells with CD34⁺/CD1a⁻ cells corresponding to the ETP stage (Figure 5B). To further reduce the number of low confidence DMRs and to characterize a robust set of DMRs in our data set, we excluded DMRs with differences in methylation patterns between ETPs, CD4⁺/NPM-ALK⁺ cells, and primary ALCL NPM-ALK⁺ cells. Two hundred forty-three DMRs (47.6%) overlapped with ETPs, CD4⁺/NPM-ALK⁺ models, and primary ALCL NPM-ALK⁺ cells. ETP cells and CD4⁺/NPM-ALK⁺ or primary NPM-ALK⁺ tumor cells shared 151 and 173 DMRs, respectively, with similar methylation patterns whereas 67 DMRs with similar methylation patterns were shared by the NPM-ALK⁺ cells, i.e., NPM-ALK–transformed CD4⁺ cells and patient-derived NPM-ALK⁺ lymphoma cells (Table 1). Primary NPM-ALK⁺ ALCL shared 72 DMRs with similar methylation patterns with ETPs (Figure 6). Using hg19 as genome reference, we identified 36 DMR-associated genes that were essentially hypomethylated (n = 30, 83%) (Table 2). Moreover, altogether, the early thymic precursors and both NPM-ALK⁺ tumor cell entities (CD4⁺/NPM-ALK⁺ lymphoma cells and primary NPM-ALK⁺ ALCL cells), shared 38 DMRs with similar methylation patterns (Figure 6). The major fraction harbor a low level of DNA methylation (n = 25, 86%) and from the 38 DMRs, using hg19 as genome reference, we identified 29 DMR-associated genes (Table 3). All together, these data suggest that, as in NPM-ALK⁺ ALCL primary tumors, NPM-ALK–transformed mature CD4⁺ cells are globally hypomethylated but also that their methylome shares close similarity with that of thymic progenitors.

Transcriptional patterns link NPM-ALK ectopic expression in normal CD4⁺ T lymphocytes and ALK⁺ anaplastic large cell lymphoma cells to early thymic progenitor cells. To complete our approach, we conducted an analysis to identify a transcription profile that showed differential expression between each thymic develop-

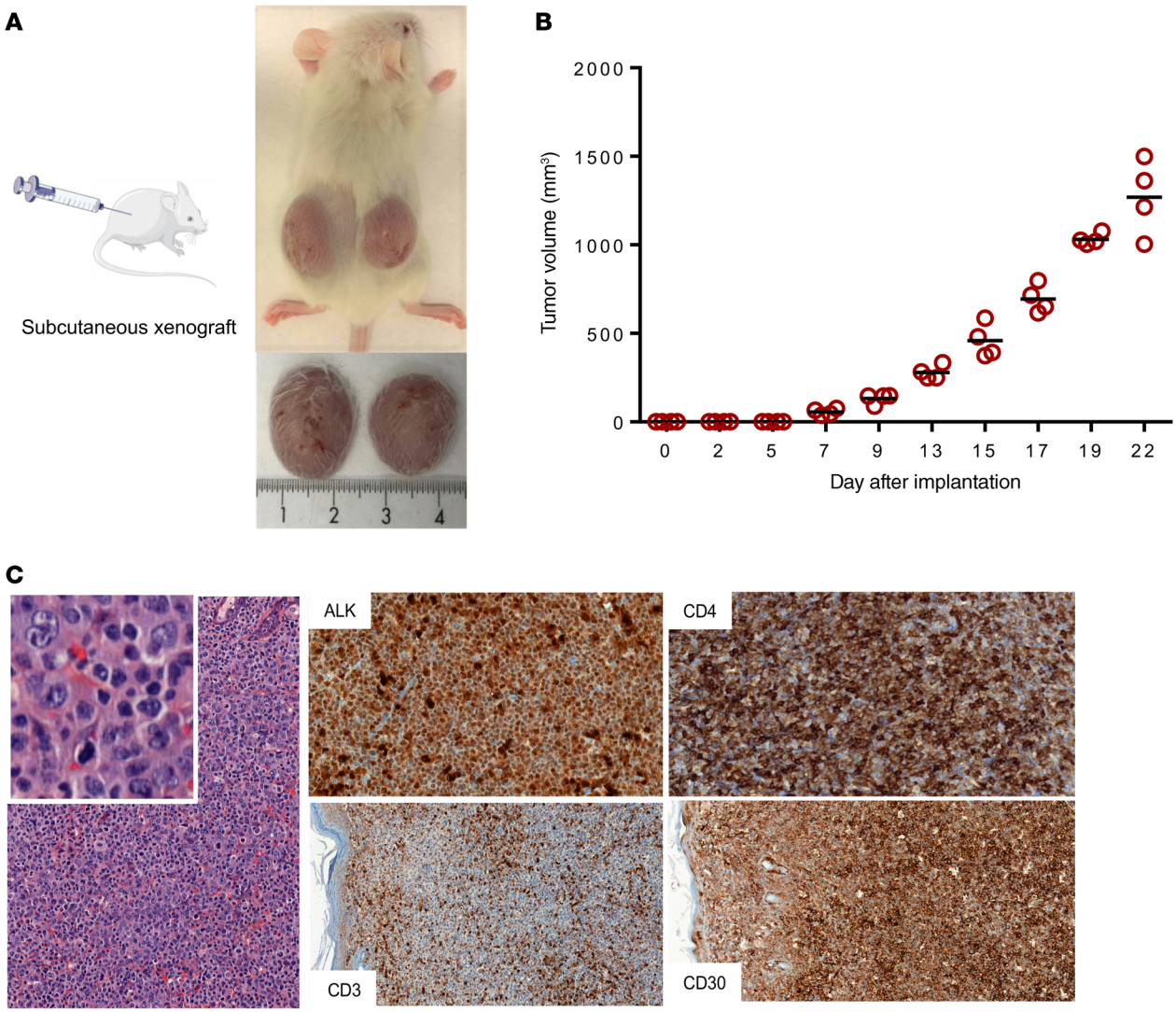

Figure 3. Growth of NPM-ALK–transformed CD4⁺ T cells in vivo. (**A**) NPM-ALK–transformed CD4⁺ T cells were injected subcutaneously into the left or right flank of NSG mice (n = 2). Representative image of tumor-bearing mice. (**B**) Tumor volume was evaluated over time by caliper measurements and reported as mean ± SEM (line). (**C**) Representative images of H&E staining and immunohistochemical staining for expression of NPM-ALK, CD3, CD4, and CD30 (original magnification ×20 or ×40; inset ×80).

mental stage. For this purpose, we generated mRNA expression profiles from several cell populations isolated ex vivo from the neonatal human thymus, which were defined in vivo maturation stages: multipotent ETPs (CD34⁺/CD1a⁻/CD7⁻; n = 3), late thymic precursor (CD34⁺/CD1a⁻/CD7⁺; n = 3), T cell–committed progenitors (CD34⁺/CD1a⁻/CD7⁺; n = 3), CD3⁻/CD4⁺ immature single-positive (ISP-CD4⁺, n = 4), CD4⁺/CD8⁺ double-positive TCR⁻ cells (DP-TCR⁻; n = 3), and TCR-expressing CD4⁺/CD8⁺ double-positive T cells (DP-TCR⁺, n = 3) (Supplemental Figure 9). Next, we integrated these data with our previous findings of gene expression array data of 55 primary NPM-ALK⁺ ALCL samples (24) and RNA-Seq data from the CD4⁺/NPM-ALK⁺ models (n = 9). First, we identified a cluster of 3628 genes that could be used to discriminate the distinct thymic populations. With regard to these 3628 genes, Pearson's correlation coefficient was calculated between NPM-ALK–transformed CD4⁺ cells or NPM-ALK⁺ lymphoma cells and each developmental T cell stage. As shown in Figure 7, we first observed that the expression of the 3628 gene set in CD4⁺/NPM-ALK⁺ models was similar to the NPM-ALK⁺ primary ALCL transcriptome (Pearson's correlation coefficient: 0.67, Table 4). Second, we observed that the gene set in NPM-ALK⁺ cells, i.e., NPM-ALK–transformed CD4⁺ cells and NPM-ALK⁺ lymphoma cells, was similar to the CD34⁺/CD1a⁻ cell transcriptome corresponding to the ETP stage (Pearson's correlation coefficients: 0.539 and 0.66, respectively, Table 4). This result was consistent with our DNA methylome data. To exclude the possibility that our unsupervised hierarchical clustering could be biased using only thymic cell populations, we used principal component analysis (PCA) to perform a comparative analysis in silico of CD4⁺/NPM-ALK⁺ transduced cells and ALCL ALK⁺ primary biopsies with a series of multi or oligopotent hematopoietic progenitor populations from bone marrow (GSE63270; ref. 25), peripheral T cells (GSE78897; ref. 26), and the most immature CD34⁺CD1a⁻CD7⁻ subset of ETPs. As shown

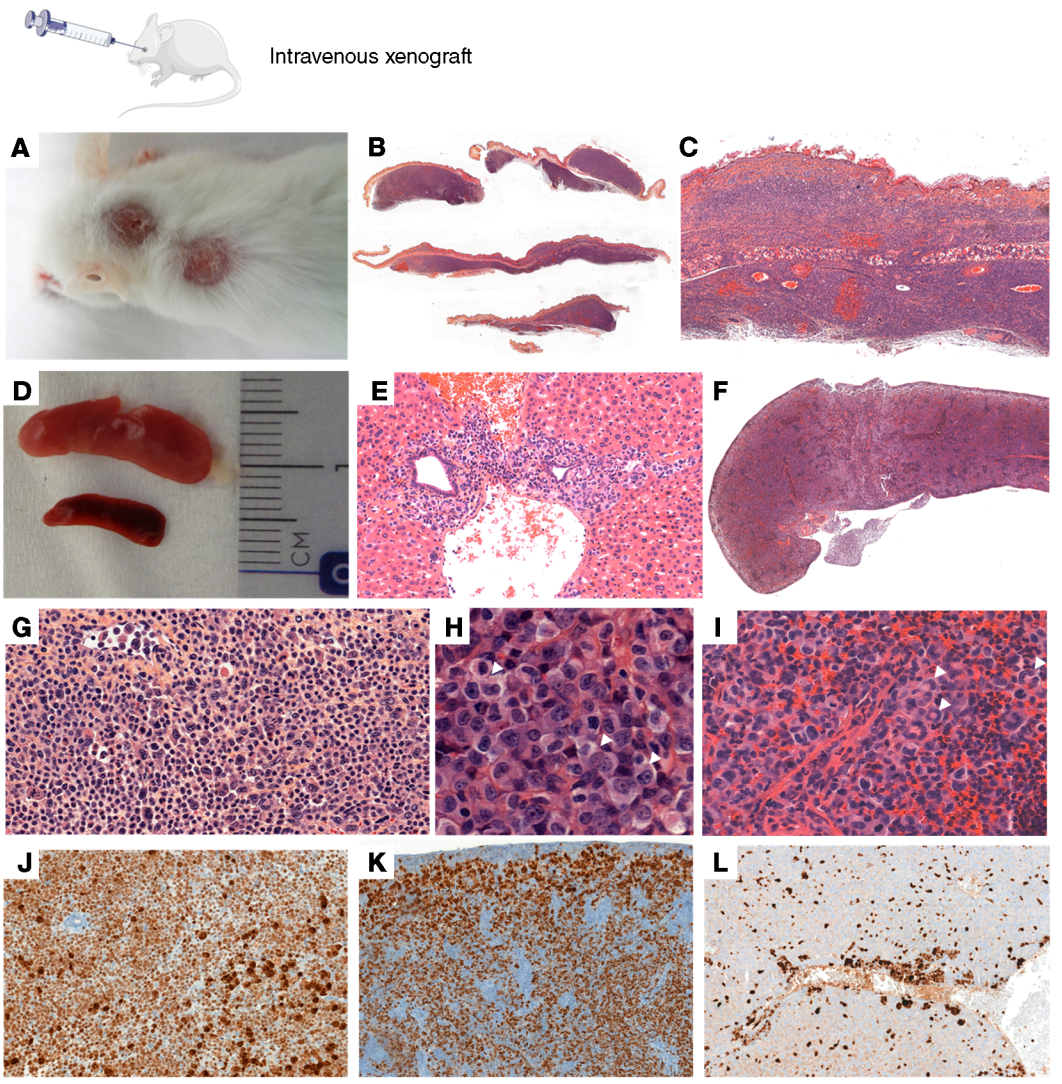

Figure 4. Experimental metastasis assays in vivo using NPM-ALK–transformed CD4⁺ T cells. Experimental metastasis assays were performed in NSG mice using NPM-ALK–transformed CD4⁺ T cells (n = 7) or PBS (n = 3) with injection through the mouse tail vein. (**A**) Representative image of cutaneous metastasis-bearing mice. Metastatic burden was assessed at 39 days after injection. (**B**–**I**) Representative H&E images. Mice presented skin nodules without dermis and subcutis hyperplasia (**A**–**C**) and spleen hyperplasia (**D**). A lymphomatous infiltration invaded the liver (**E**) and spleen (**F**). The neoplastic cells included a predominant population of small- to medium-sized neoplastic cells with irregular nuclei (**G**). Many cells are fried-egg cells with pale cytoplasms and centrally located nuclei (**H**, arrowheads) and cells with ring-like nuclei (**I**, arrowheads). Histological analysis with anti-ALK antibody showed a strong ALK staining in the large lymphoma cells as compared with the small variants (**J** and **K**). Small cells are often localized around blood vessels (**L**). Original magnifications ×5, ×20, or ×40).

in Supplemental Figure 10, PCA analysis revealed a clear separation of ALK⁺ samples and hematopoietic progenitor populations from bone marrow along PC1. In addition, along PC2, all ALK⁺ samples were proximate to normal peripheral cells including ILC3 and Th17 cells, as previously described (27), with a stronger skewing toward an ETP profile, consistent with our unpublished data. Taken together, these results confirm that CD4⁺/NPM-ALK⁺–transduced cells and cells from ALCL ALK⁺ primary biopsies exhibit ETP-like gene expression profiles.

Moreover, in the cluster of 3628 genes that could be used to discriminate the distinct thymic populations, 987 genes shared a similar expression pattern in NPM-ALK⁺ lymphoma primary cells and ETPs. In support of this, besides our data from methylation and transcriptomic analysis, we analyzed the expression of transcription factors required for the early stages of thymocyte maturation (*TCF7*, *BCL11B*, and *LEF1*) and associated to pluripotency (*OCT4*, *SOX2*, *NANOG*). Using *ALB*, *MLN51*, *5S*, *GAPDH*, *S14*, and *RLP0* genes for normalization, and qRT-PCR in CD4⁺/NPM-ALK⁺ (n = 9) and NPM-ALK⁺ ALCL (n = 29), we observed the significantly lower expression levels of transcriptional drivers of the T cell lineage program (*TCF7*, *BCL11B*, and *LEF1*) (Supplemental Figure 11) and the overexpression of regulators of stem cell features (*OCT4*, *SOX2*, and *NANOG*) in NPM-ALK⁺ cells compared with preactivated healthy activated CD4⁺ lymphocytes (n = 5) (Supplemental Figure 12). Of note, we also detected promoter DNA hypermethylation of *TCF7*, *BCL11B*, and *LEF1* in CD4⁺/NPM-ALK⁺ cells compared with stimulated normal CD4⁺ T cells using our DNA methylation data sets (Supplemental Figure 13).

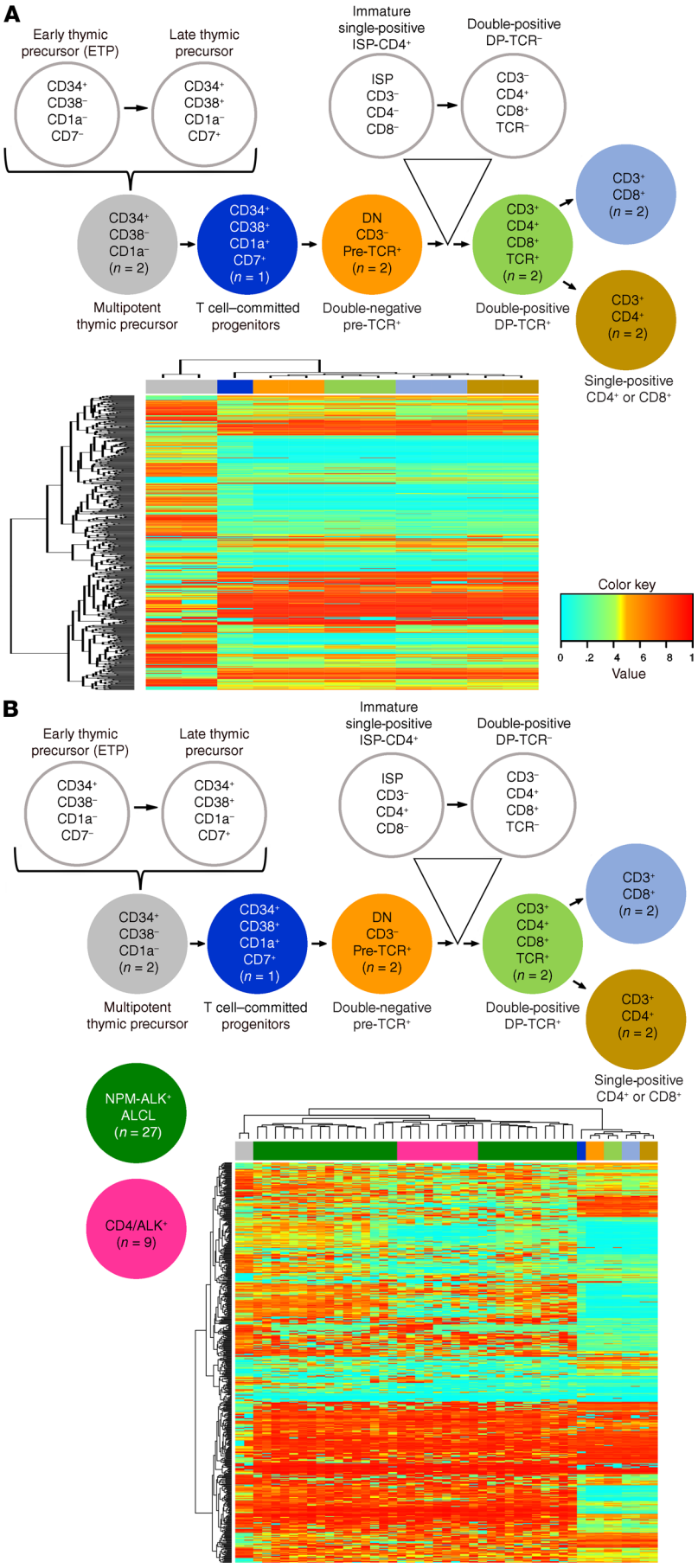

Figure 5. DMRs revealed that NPM-ALK–transformed CD4⁺ T cells and primary NPM-ALK⁺ ALCL cells have a close similarity with the ETP. (**A**) We used publicly available methylation data sets (30) generated from different developmental T cell stages (multipotent ETPs [CD34⁺/CD1a⁻; *n* = 2]; T cell–committed progenitors [CD34⁺/CD1a⁺; *n* = 1]; pre-TCR T cells [*n* = 2]; TCR-expressing CD4⁺/CD8⁺ double-positive T cells [DP-TCR⁺, *n* = 2]; and single positive [SP] CD8⁺ or CD4⁺ cells [SP-CD4⁺; *n* = 2 or SP-CD8⁺; *n* = 2]) to identify a cluster of 510 DMRs available to discriminate each different stage of T cell differentiation in the thymus. (**B**) Hierarchical clustering dendrogram using a cluster of 510 DMRs revealed that NPM-ALK–transformed CD4⁺ T cells were distant to the healthy CD4⁺ lymphocyte profile and clustered with primary NPM-ALK⁺ ALCL biopsies. Heatmaps also showed a similarity of NPM-ALK⁺ cells (NPM-ALK–transformed CD4⁺ T cells and primary patient-derived NPM-ALK⁺ ALCL) with CD34⁺/CD1a⁻ cells corresponding to the ETP stage.

Altogether, these data suggested that in NPM-ALK–transformed mature CD4⁺ lymphocytes, the oncogenic tyrosine kinase ALK induces mRNA and methylation patterns related to a conversion toward progenitor cell features.

NPM-ALK is responsible for HIF2A expression in lymphoma cells. Among the 987 genes sharing similar expression patterns in NPM-ALK⁺ lymphoma primary cells and ETPs, using the methylome data sets from both NPM-ALK⁺ lymphoma T cell entities (NPM-ALK–transformed CD4⁺ cells [*n* = 9] and patient-derived NPM-ALK⁺ lymphoma cells [*n* = 22]), we were able to extract the DNA methylation status for 266 genes: 168 of 266 genes were hypomethylated and 98 of 266 genes were hypermethylated. Finally, we overlapped these data with the 29 genes related to 38 DMRs with similar expression patterns in 3 cell entities: NPM-ALK–transformed CD4⁺ lymphocytes, patient-derived NPM-ALK⁺ lymphoma cells, and ETPs. We noted a hypomethylated status for 22 genes (*ANAPC10*, *ANGPT1*, *BAHCC1*, *C11orf77*, *CACNA2D4*, *CAPZB*, *CDC25B*, *CLEC16A*, *EPAS1*, *DIABLO*, *GLTSCR2*, *IQCH*, *KLF7*, *NARS2*, *PLCH1*, *RASA3*, *SCP2*, *SLC25A25*, *SLC7A11*, *SNORD23*, *ZHX2*, *ZNF516*) and a hypermethylated status for 3 genes (*ARHGEF10*, *MRLP41*, *ITGAX*) (Table 3). To validate this signature, qRT-PCR using high-throughput Fluidigm technology was performed on primary NPM-ALK⁺ ALCL (*n* = 29) and CD4⁺/NPM-ALK⁺ models (*n* = 7). Nine of the 26 genes (*ANGPT1*, *BAHCC1*, *C11orf77*, *EPAS1*, *IQCH*, *ITGAX*, *PLCH1*, *SCP2*, and *ZNF516*) gave concordant results with an adjusted *P* value of less than 0.05 compared with activated healthy CD4⁺ lymphocytes (*n* = 5) with the 6 genes used for normalization: *ALB*, *MLN51*, *5S*, *GAPDH*, *S14*, and *RLP0* (data not shown). Among these 9 genes, we focused our attention on the *EPAS1* gene (endothelial PAS domain protein 1) (Figure 8A) which encodes the transcriptional activator HIF-2α, which

Table 1. Similar methylation patterns

DMRs sharing similar expression pattern	CD4⁺/NPM-ALK⁺ and ETPs	Primary ALCL NPM-ALK⁺ and ETPs	Primary ALCL NPM-ALK⁺ and CD4⁺/NPM-ALK⁺
243/510	151/243	173/243	67/243

Similar expression patterns were shared by 243 among the 510 DMRs within NPM-ALK–transformed CD4⁺ T cells (CD4⁺/NPM-ALK⁺), primary patient–derived NPM-ALK⁺ ALCL, and CD34⁺/CD1a⁻ cells corresponding to the ETP stage. ETP cells and CD4⁺/NPM-ALK⁺ or primary NPM-ALK⁺ tumor cells shared 151 and 173 DMRs with similar expression patterns, respectively, while 67 DMRs with similar expression patterns were shared by the NPM-ALK⁺ cells (NPM-ALK–transformed CD4⁺ T cells and primary patient–derived NPM-ALK⁺ ALCL).

activates OCT4, SOX2, and NANOG expression (28–30). However, in NPM-ALK⁺–transformed CD4⁺ cells, siRNA-mediated HIF2α knockdown did not affect mRNA and protein levels of factors associated with pluripotency (*OCT4*, *SOX2*, and *NANOG*) compared with cells transfected with a negative control miRNA (miR-CTL) (Supplemental Figure 14).

NPM-ALK activity drives HIF2A expression in lymphoma cells. In an attempt to elucidate the mechanisms involved in HIF2A expression in NPM-ALK⁺ cells, first as an assessment of the putative functional role of STAT3 in HIF2A expression, we used FIMO (find individual motif occurrences) software to identify 3 putative DNA motif logos in the STAT3 consensus sequence of the *EPAS1* gene promoter (–2000 to +2375 around the TSS). Second, employing both the KARPAS-299 cell line and NPM-ALK–transformed CD4⁺ cells, we used q-CHIP experiments to analyze the association of STAT3 with the *EPAS1* gene. As shown in Supplemental Figure 15, no STAT3 binding was observed. Third, we checked whether NPM-ALK could itself be involved in *EPAS1* expression by qRT-PCR, using *ALB*, *MLN51*, *5S*, *GAPDH*, *S14*, and *RLP0* genes for normalization and in comparison with activated healthy CD4⁺ lymphocytes ($n = 5$). We observed that *EPAS1* mRNA levels were significantly increased concomitantly to ALK mRNA expression in primary patient–derived NPM-ALK⁺ ALCL cells ($n = 29$) (Figure 8A). Moreover, either NPM-ALK expression or catalytic activity was silenced in 3 human NPM-ALK⁺ ALCL cell lines (KARPAS-299, COST, and SU-DHL-1) and in 1 CD4⁺/NPM-ALK⁺ model using siRNAs directed against *ALK* mRNA and the ALK inhibitor crizotinib, respectively (Figure 8B). We observed that both HIF2A mRNA and protein levels were decreased in all NPM-ALK⁺ cell lines upon ALK inhibition. In addition, we assessed the role of STAT3, a key ALK effector, in the regulation of HIF2A. We knocked down STAT3 in the 4 NPM-ALK⁺ cell lines, using siRNAs directed against *STAT3* mRNA and observed that the depletion of STAT3 was concomitantly correlated with a codepletion of HIF2A (Figure 8B) and tumor cell growth alteration (Supplemental Figure 1B and Supplemental Figure 2B). Altogether, these results suggest that in NPM-ALK–transformed mature CD4⁺ lymphocytes, HIF2A expression is essential for tumor growth and that ALK tyrosine kinase activity and STAT3 regulate HIF2A expression.

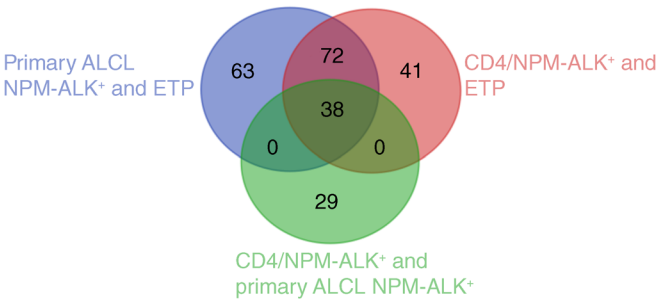

Figure 6. DMRs of NPM-ALK–transformed CD4⁺ T cells and primary patient–derived NPM-ALK⁺ ALCL cells and the ETP. Two hundred and forty-three among the 510 DMRs within NPM-ALK–transformed CD4⁺ T cells (CD4⁺/NPM-ALK⁺), primary patient–derived NPM-ALK⁺ ALCL cells, and CD34⁺/CD1a⁻ cells corresponding to the ETP stage. Venn diagram reveals that the ETP and both the NPM-ALK⁺ tumor cell entities (CD4⁺/NPM-ALK⁺ lymphoma cells and primary NPM-ALK⁺ ALCLs) share 38 DMRs with similar expression patterns.

Discussion

The hallmark of NPM-ALK⁺ ALCL is the expression of the CD30 antigen, whose upregulation in healthy activated T cells requires the CD3/TCR complex and is observed upon several stimuli such as antigen stimulation in vivo and anti-CD3 or cytokine signalling in vitro (31, 32). Our study shows that after preactivation, NPM-ALK–transduced normal CD4⁺ mature T cells (CD4⁺/NPM-ALK⁺) become immortalized and acquire a surface phenotype that is identical to systemic NPM-ALK⁺ ALCL, including expression of CD30, partial loss of TCR, CD3, CD2, CD5, and CD7, along with the maintenance of CD4 expression. Tissue examination of the tumors formed by NPM-ALK–transduced normal CD4⁺ mature T cells xenotransplanted into immunodeficient mice revealed their striking resemblance to patient NPM-ALK⁺ ALCL. Integrating genome-wide DNA methylation, and transcriptome analysis, we observed high degrees of similarity between our CD4⁺/NPM-ALK⁺ models and patient-derived NPM-ALK⁺ ALCL. Our results are in agreement with those obtained by Zhang et al, which show that NPM-ALK expression in mature CD4⁺ T lymphocytes has the capacity to induce various changes in terms of morphology and phenotype reminiscent of those observed in primary NPM-ALK⁺ ALCL (15). In addition, we reinforced our previous observations, which indicated that NPM-ALK is sufficient to significantly induce tumor lymphocyte survival and promote metastasis formation (17).

Although NPM-ALK⁺ ALCLs are historically believed to derive from peripheral mature CD4⁺ CD30⁺ T cells, the cellular origin of ALCL is still in debate. Recent studies suggested that the cell of origin could be an immature thymic precursor cell with stem-like properties (6, 10, 11). TCR rearrangements could be used by thy-

Table 2. Similar expression patterns of 72 DMRs in primary NPM-ALK$^+$ ACLCs and ETPs

Gene symbol	DNA methylation status
ABR	Hypomethylation
ADCK4	Hypomethylation
AMBRA1	Hypomethylation
BCL11B	Hypermethylation
CARS	Hypomethylation
CHRNA3	Hypomethylation
CUL3	Hypomethylation
DENND2A	Hypomethylation
DYNC1H1	Hypomethylation
EFHD2	Hypomethylation
EHD2	Hypomethylation
FOXP1	Hypomethylation
GNAS	Hypomethylation
HECW16	Hypomethylation
IGF1R	Hypomethylation
ITGAE	Hypomethylation
KIAA1199	Hypomethylation
KIR2DS4	Hypomethylation
LCK	Hypomethylation
MAD1L1	Hypomethylation
NINJ2	Hypomethylation
PCK2	Hypomethylation
PIGG	Hypomethylation
PNLIPRP2	Hypomethylation
RNASE13	Hypermethylation
RUNX2	Hypermethylation
SIGLEC1	Hypermethylation
SLC25A33	Hypomethylation
SMAD3	Hypomethylation
SNTG2	Hypomethylation
STARD3NL	Hypomethylation
STON1-GTF2A1L	Hypomethylation
SULF2	Hypermethylation
SYNJ2	Hypomethylation
TMEM91	Hypermethylation
TSPAN14	Hypomethylation

Primary NPM-ALK$^+$ ALCLs and ETPs share 72 DMRs with similar expression patterns. Using hg19 as genome reference, 36 DMRs were associated with a gene. The major fraction was hypomethylated.

Table 3. Similar expression patterns of 38 DMRs in NPM-ALK$^+$ tumor cell entities and ETPs

Gene symbol	DNA methylation status
ANAPC10	Hypomethylation
ANGPT1	Hypomethylation
ARHGEF10	Hypermethylation
ARPP-21	Hypomethylation
ASAM	Hypomethylation
BAHCC1	Hypomethylation
C11orf77	Hypomethylation
C6orf145	Hypermethylation
CACNA2D4	Hypomethylation
CAPZB	Hypomethylation
CDC25B	Hypomethylation
CLEC16A	Hypomethylation
DIABLO	Hypomethylation
EPAS1	Hypomethylation
GLTSCR2	Hypomethylation
IQCH	Hypomethylation
ITGAX	Hypermethylation
KLF7	Hypomethylation
MRPL41	Hypermethylation
NARS	Hypomethylation
PLCH1	Hypomethylation
RAG2	Hypomethylation
RASA3	Hypomethylation
SCP2	Hypomethylation
SLC25A25	Hypomethylation
SLC7A11	Hypomethylation
SNORD23	Hypomethylation
ZHX2	Hypomethylation
ZNF516	Hypomethylation

NPM-ALK$^+$ tumor cell entities (CD4$^+$/NPM-ALK$^+$ lymphoma cells, primary NPM-ALK$^+$ ALCL) and ETPs share 38 DMRs with similar expression patterns. Using hg19 as genome reference, 29 DMRs were associated with a gene. The major fraction was hypomethylated.

mic ALK$^+$ cells to leave the thymus and be subsequently downregulated in the periphery to allow ALK-mediated transformation and proliferation (6). In support of this thymic origin, a cell population expressing the immature cell surface marker CD44 was observed in the transgenic murine model expressing NPM-ALK under the CD4 promoter. This CD44 population gave rise to thymic CD30$^+$ CD4$^+$ NPM-ALK$^+$ tumors when transplanted intravenously into recipient mice, again in keeping with an early thymic origin. Although CD44 expression is normally restricted to immature thymocytes, its expression is probably not a remnant of expression on immature T cells because NPM–ALK is capable of driving expression of luciferase from the CD44 promoter (6). Moreover, NPM-ALK$^+$ ALCL cell lines and tumors (a) revealed close similarity between the NPM-ALK$^+$ ALCL methylome and that of thymic progenitors (10, 22), (b) expressed pluripotency-associated proteins, and (c) were enriched in a gene expression profile consistent with early thymic progenitors (11). For what we believe is the first time, using DNA methylation and transcriptomic data we linked NPM-ALK–transduced normal CD4$^+$ mature T cells and NPM-ALK$^+$ ALCL biopsies to early T cell precursors.

As any CD3 activated cells can express detectable CD30 surface molecules, it may be tempting to speculate that TCR activated cells could be easily transformed by NPM-ALK. Alternatively, NPM-ALK lentiviral preparations could also efficiently transduce rare naive circulating CD30$^+$ cells such as thymocytes. To reinforce our results, using human umbilical cord blood–derived (UCB-derived) CD34$^+$CD38^{lo} stem cells and a 3D artificial thymic organoid culture system in vitro, we differentiated these immature hematopoietic cells into functional, mature naive T lymphocytes closely resembling naive (without antigen stimulation) mature T cells from the thymus and blood (33, 34). This optimized artificial thymic organoid system induced rapid and efficient T lin-

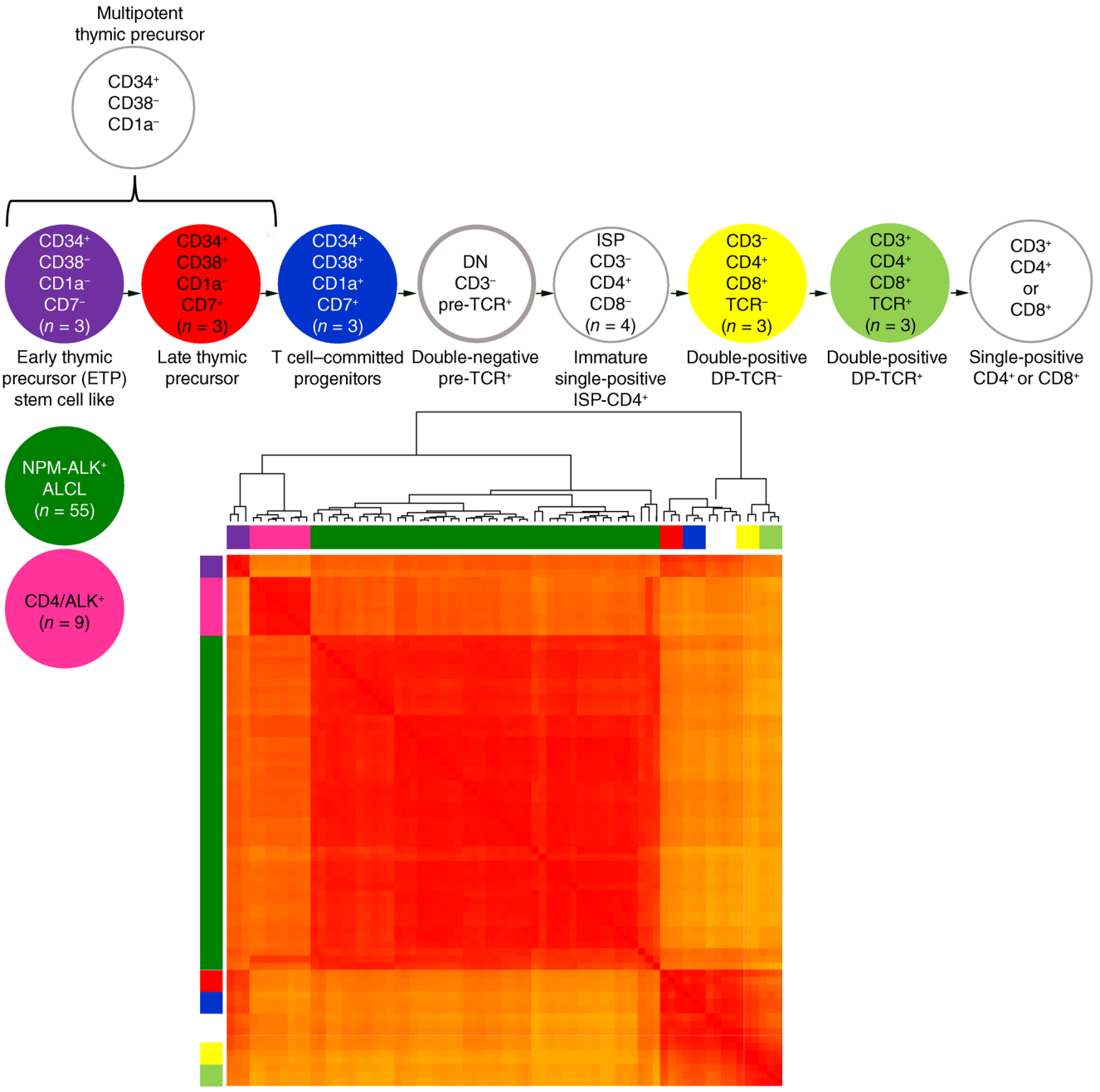

Figure 7. Transcriptional pattern links NPM-ALK–transformed CD4+ T cells and primary patient–derived NPM-ALK+ ALCL cells to ETP cells. mRNA expression profiles from several cell populations isolated ex vivo from the neonatal human thymus defining in vivo maturation stages, multipotent ETPs (CD34+/CD1a−/CD7−; *n* = 3), late thymic precursor (CD34+/CD1a−/CD7+; *n* = 3), T cell–committed progenitors (CD34+/CD1a−/CD7+; *n* = 3), CD3−/CD4+ immature single-positive (ISP) (ISP-CD4+, *n* = 4), CD4+/CD8+ double-positive TCR− cells (DP-TCR−; *n* = 3), and TCR-expressing CD4+/CD8+ double-positive T cells (DP-TCR+, *n* = 3) were integrated with our previous findings from the gene expression array data of 55 primary NPM-ALK+ ALCL samples (NPM-ALK+ ALCL) (35) and RNA-Seq data from the NPM-ALK–transformed CD4+ T cells (CD4+/NPM-ALK+; *n* = 9). NPM-ALK CD4+/NPM-ALK+ cells were distant to the healthy CD4+ lymphocyte but close to NPM-ALK+ ALCL. Moreover, NPM-ALK+ cells (NPM-ALK–transformed CD4+ T cells and primary patient–derived NPM-ALK+ ALCL) showed a similarity with the ETP stage.

eage commitment from UCB CD34+CD38lo cells, as shown by the emergence of mature CD3+/CD4+/TCR+ cells including rare CD30+ cells (Supplemental Figure 16). Using the same strategy, we generated T cells expressing the NPM-ALK oncogene and we observed the emergence of rare CD4+/CD3−/TCR−/CD30+ lymphocytes (Supplemental Figure 16). In vivo, no tumors were observed in NGS mice xenografted with these naive CD4+/CD3−/TCR−/CD30+/NPM-ALK+ T lymphocytes even 10 months after intravenous injection (Supplemental Figure 16). Our data suggest that NPM-ALK lentiviral preparations can efficiently transduce rare CD30+ naive T cells from the thymus and blood, but in the absence of antigen stimulation we suggested that this was not sufficient to allow cell transformation. These data could crosstalk with previously reported data that showed circulating t(2;5)+ cells

can be detected in the cord blood of newborn babies, which contains adult stem cells that mature into healthy blood cells (35–37).

By comparing gene expression signatures derived from normal human hematopoietic stem cells and progenitor thymocytes, gene set enrichment analysis suggested that NPM-ALK$^+$ ALCL cell lines presented an enriched gene expression profile associated with ETPs. Our signature from NPM-ALK–transduced normal CD4$^+$ mature T cells as from NPM-ALK$^+$ ALCL biopsies was also enriched in pluripotency-associated transcription factors such as OCT4, SOX2, and NANOG, which can be activated by the transcriptional activator HIF2A (11, 38). HIF2A, encoded by the *EPAS1* gene, plays a major role in the maintenance of undifferentiated states (39). In ALCL lymphoma cells, HIF2A is regulated by NPM-ALK via STAT3 and is essential for tumor growth (14). We observed that in contrast to stimulated normal CD4$^+$ T lymphocytes, mature CD4 transformed with the NPM-ALK oncogene, and NPM-ALK$^+$ lymphoma biopsies overexpressed the *EPAS1* gene. In CD4$^+$/NPM-ALK$^+$ lymphoma cells, HIF2A expression is dependent on both ALK tyrosine kinase and STAT3 activities. HIF2A silencing upon depletion of NPM-ALK or STAT3 activity suppressed cell growth of NPM-ALK transformed CD4$^+$ lymphocytes.

Altogether, our findings suggest that NPM-ALK could transform mature CD30$^+$CD4$^+$ peripheral T lymphocytes. These cells were enriched in features similar to the ETP stage of thymic development, suggesting that the progenitor phenotype of ALK$^+$ ALCL may be dictated by the ALK fusion and might not be related to the putative thymic origin of these neoplasms (Supplemental Figure 17).

Methods

Additional methods can be found in Supplemental Methods.

Human cell lines and tumoral and normal samples. CD4$^+$ T cells were purified with human CD4 MicroBeads (Miltenyi Biotec) from human PBMCs isolated using density gradient centrifugation with Ficoll-Paque Plus (Thermo Fisher Scientific). PBMCs were obtained from healthy donor blood samples provided by the therapeutic innovations in B lymphoma team (Cancer Research Center of Toulouse, France). The human NPM-ALK$^+$ ALCL cell line COST was established in the laboratory (40) and KARPAS-299 and SU-DHL-1 NPM-ALK$^+$ ALCL cell lines were obtained from DSMZ (German Collection of Microorganisms and Cell Culture, Braunschweig, Germany). Cells were cultured in RPMI-1640 supplemented with FCS according to Congras et al. (41). NPM-ALK$^+$ ALCL tumor samples were registered at the CRB cancer des Hôpitaux de Toulouse. Clinical data from NPM-ALK$^+$ primary samples (ALCL 1, 4, 5, 6, 7, 9, 10, 11, 12, 18, 19, 22, 24, 25, 26, 27, 29, 30, 31, 35, 36, 37, 38, 39, 40, 42, 43, 51, 52, 53, 55, 56, 57, 59, 62, 63, 64, 67, 74, 81, 82) came from our laboratory and some of them were previously described by Malcom et al. (6). A member of our research team generated Infinium HumanMethylation450 BeadChip raw data from 5 primary NPM-ALK$^+$ ALCLs previously published in Cell Reports (10). Control tissue samples, lymph nodes from patients with reactive nonmalignant disease, were provided by the CRB-Cancer du CHU de Bordeaux BRIF BB-0033-00036 (member of the Cancéropôle Grand Sud-Ouest network).

Lentiviral transduction of CD4$^+$ T lymphocytes. The pTRPE-NPM-ALK lentivirus was provided by J. Riley (University of Pennsylvania, Perelman School of Medicine, Philadelphia, Pennsylvania, USA) and has been previously described (15). The lentivirus was produced by the TBMCore facility (CNRS UMS 3427, INSERM US 005, University of Bordeaux, Bordeaux, France). CD4$^+$ T cells were activated with magnetic anti-CD3/28 antibody-coated beads at a 1:3 cell/bead ratio (Dynabeads human T-activator CD3/CD28; Thermo Fisher Scientific). Transductions with lentiviral vectors (expressing NPM-ALK/GFP or GFP alone) were performed in 24-well plates precoated with retronectine. Fresh medium was added to the cells every 2 days. On day 5, the magnetic CD3/CD28 antibody-coated beads were removed.

Drug treatment and siRNA transfection. Human NPM-ALK$^+$ cell lines and CD4$^+$/NPM-ALK$^+$ cells were treated for up to 72 hours with crizotinib (@rtMolecule) at 500 nM (PBS as vehicle control). Transfection with 20 nmol siRNA molecules si-ALK (GGGCGAGCUACUAUAGAAA), si-STAT3 (AACAUCUGCCUAGAACGGCUA), siEPAS1 SMART Pool On Target (Dharmacon, catalog L-004814-00-0020), or si-CTL Smart Pool 4609 (Dharmacon) (negative control) were performed by electroporation (Bio-Rad Gene Pulser) at 250 V, 950 μF, 100 Ohms.

RNA extraction and qRT-PCR for gene expression analysis. Total fraction of RNA from NPM-ALK$^+$ cell lines and CD4$^+$ T cells was prepared using the TRIzol reagent (Ambion) or with an AllPrep DNA/RNA/miRNA universal kit (Qiagen), according to the manufacturer's instructions. RNA (200 ng) was reverse-transcribed with the QuantiTect Reverse Transcription kit (Qiagen), according to the manufacturer's protocol. Quantitative PCR was performed using SYBR Premix Ex Taq (Tli RNaseH plus) on the StepOnePlus apparatus (Applied Biosystems). Respectively, the forward and reverse primers used were as follows: for NPM/ALK-F (5′-CAGTGCATATTAGTGGACAGCTAG-3′) NPM/ALK-R (5′-TGATGGTCGAGGTGCGGA-3′); for GAPDH-F (5′-CGGGAAGCTTGTGATCAATGG-3′) GAPDH-R (5′-GGCAGTGATGGCATGGACTG-3′); for MLN51-F (5′-TAATCCCAGTTACCCTTATGCTCCA-3′) MLN51-R (5′-GTTAATAGTAGGTCACTCCTCCATATACCTGT-3′); for EPAS1-F (5′GGCCACAGCGACAATGACAGC-3′) EPAS1-R (5′-CCTCCGTCTCCTTGCTCCGC-3′); for OCT4-F (5′-CAGCCACATCGCCCAGCA-3′) OCT4-R (5′-AGAAAGGAGACCCAGCAGCCT-3′); for SOX2-F (5′-ATGGGTTCGGTGGTCAAGTCC-3′) SOX2-R (5′-TGT-

Table 4. Pearson's correlation coefficient to discriminate cell population

Cells	Pearson's correlation coefficient	
ETPs	0.660	0.539
Late thymic precursor	0.562	0.532
T cell–committed progenitors	0.514	0.495
ISP-CD4$^+$	0.502	0.539
DP TCR$^-$	0.449	0.488
DP TCR$^+$	0.441	0.49
NPM-ALK$^+$ ALCL	1	0.670
CD4$^+$/NPM-ALK$^+$	0.670	1

Using a cluster of 3628 genes that discriminate the distinct thymic populations, Pearson's correlation coefficient (*r*) was calculated between CD4$^+$/NPM-ALK$^+$ cells ($r = 1$) or primary NPM-ALK$^+$ ALCL ($r = 1$) and each developmental T cell stage and revealed that (a) NPM-ALK CD4$^+$/NPM-ALK$^+$ cells were distant to the healthy CD4$^+$ lymphocyte but close to NPM-ALK$^+$ ALCL and (b) showed a similarity of NPM-ALK$^+$ cells (NPM-ALK–transformed CD4$^+$ T cells and primary patient–derived NPM-ALK$^+$ ALCL) with ETP stage. Bold indicates the references ($r = 1$) of the analysis.

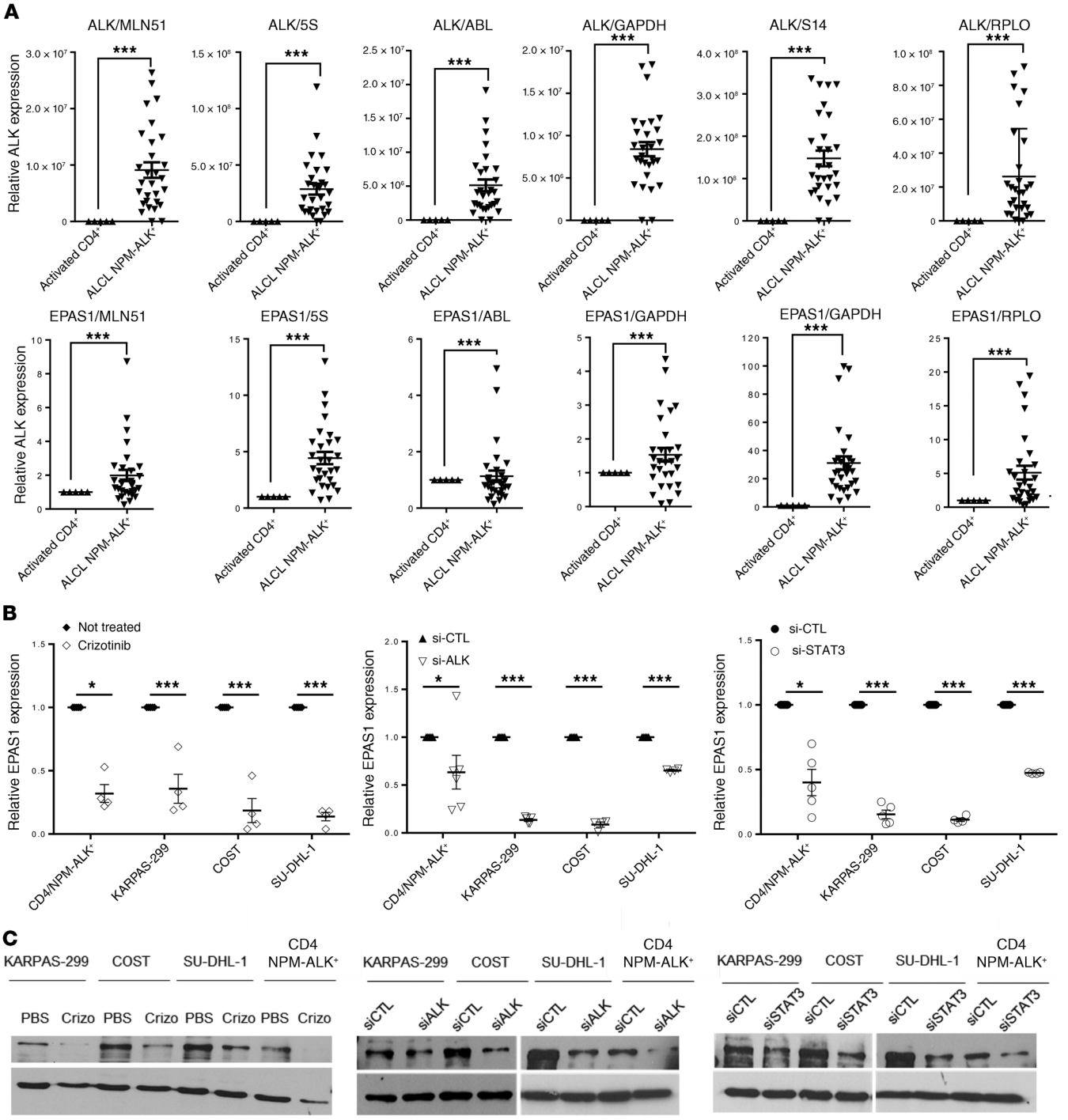

Figure 8. HIF2A, encoded by the *EPAS1* gene, is strictly dependent on NPM-ALK activity and activation of the STAT3 key signal transduction pathways in lymphoma cells. (**A**) Quantitative RT-PCR analysis of ALK and EPAS1 mRNA was performed in primary patient–derived NPM-ALK$^+$ ALCL cells (n = 29). Relative mRNA expression was expressed as the 2–ΔΔCt relative to MLN51, S5, ABL, GAPDH, S14, or RPLO genes for normalization and compared with pre-activated healthy CD4$^+$ lymphocytes (n = 5). Data represent mean ± SEM. ***P < 0.001; unpaired 2-tailed Student's t test. (**B**) Quantitative RT-PCR analysis of EPAS1 mRNA expression in NPM-ALK$^+$ lymphoma cell lines, COST, KARPAS-299 (KARPAS), and SU-DHL1, treated for 72 hours or not (PBS) with crizotinib or transfected with either an irrelevant siRNA as the negative control (si-CTL) or a siRNA targeting ALK mRNA (si-ALK) or STAT3 (si-STAT3). Relative EPAS1 mRNA expression was expressed as the 2–ΔCt relative to MLN51. Data represent mean ± SEM from 3 independent experiments. *P < 0.05, ***P < 0.001; unpaired 2-tailed Student's t test with Welch's correction. (**C**) Western blotting analysis of HIF2A expression (top) in NPM-ALK$^+$ COST, KARPAS-299, and SU-DHL1 cells treated with crizotinib (crizo) or not (PBS), transfected by si-CTL, si-ALK, or si-STAT3. The GAPDH protein (bottom) served as an internal control to ensure equal loading. Results from 1 representative experiment are shown.

GAAGTCTGCTGGGGGCG-3′); for NANOG-F (5′-ACCTATGCCTGTGATTTGTGGGC-3′) NANOG-R (5′-TGTTTGCCTTTGGGACTGGTG-3′); for TCF7-F (5′-TGCACCAGCGGCATGTACAAA-3′) TCF7-R (5′-CAGGTCCAGGGGTGGGATGT-3′); for BCL11B-F (5′-AATGTCCCGCCGCAAACAGG-3′) BCL11B-R (5′-ACCCACCATCAGCCCCAG-3′); for LEF1-F (5′-AAGGTGGCATGCCCTCTCCC3′) or LEF1-R (5′-GCTTCGTTTTCCACCTGATGCAGA-3′. Expression levels of 29 selected genes based on microarray data were studied by qRT-PCR using high-throughput Fluidigm technology.

RNA-seq procedures. Healthy CD4$^+$ T and CD4$^+$/NPM-ALK$^+$ cell libraries were prepared with NEBNext Ultra II Directional RNA Library Prep Kit for Illumina protocol according to the supplier's recommendations. Briefly, the key stages of this protocol are, successively, the purification of PolyA containing mRNA molecules using poly-T oligo attached magnetic beads from 1 μg total RNA (with the Magnetic mRNA Isolation Kit from New England Biolabs), a fragmentation using divalent cations under an elevated temperature to obtain approximately 300 bp pieces, double-strand cDNA synthesis, and finally, Illumina adapter ligation and cDNA library amplification by PCR for sequencing. Sequencing was then carried out on a 75 bp paired end on an Illumina HiSeq4000. FASTQ files were aligned and quantified using RSEM (https://deweylab.github.io/RSEM/) (RSEM 1.3.1, bowtie2-2.2.6) and the homo sapiens transcriptome reference GRCh38. Differential analysis of RNA-Seq data at the gene level was performed using the DESeq2 package (42, 43). All original microarray data were deposited in the NCBI's Gene Expression Omnibus database (GSE160123).

Protein extraction and Western blotting analyses. Cells were lysed by sonication in RIPA-buffer (20 mM Tris-HCl, 150 mM NaCl, 4 mM EDTA, 0.5% Triton X 100, and 0.2% SDS) supplemented with protease inhibitors (complete protease inhibitor cocktail tablets; Roche). After removal of the insoluble material (centrifugation for 10 minutes at 10,000*g*), total protein concentration was determined using a BCA assay. Proteins were separated using 10% SDS-acrylamide gels and transferred onto nitrocellulose membranes (Trans-Blot Turbo, Bio-Rad) according to the manufacturer's protocol. Immunodetections were performed with antibodies directed against NPM-ALK at 1/5000 (Cell Signaling, catalog 3633), phospho-ALK at 1/1000 (Cell Signaling, catalog CS14678S), STAT3 at 1/1000 (Cell Signaling, catalog CS9132), P-STAT3 at 1/1000 (Cell Signaling, catalog CS9131), HIF2α at 1/1000 (Bethyl, catalog MAB374), NANOG at 1/1000 (Cell Signaling, catalog CST 4893S; mouse mAb 1E6C4), SOX2 at 1/1000 (Cell Signaling, catalog CST 4900S; mouse mAb L1D6A2), OCT4 at 1/500 (StemGent, catalog 09-0023 rabbit polyclonal), β-tubulin at 1/5000 (MilliporeSigma, catalog T4026; mouse mAb TUB 2.1), or GAPDH at 1/10,000 (Millipore, catalog MAB374). Signals from HRP-coupled secondary antibodies were generated by the enhanced chemiluminescence solution (Chemiluminescent Peroxidase Substrate-3 Kit; MilliporeSigma) or the Clarity Western ECL Substrate (Bio-Rad).

Flow cytometry. Intracellular staining was performed using fixation and permeabilization reagents (BD Cytofix/Cytoperm, BD Biosciences) according to the manufacturer's instructions. NPM-ALK detection was performed with anti–NPM/ALK-PE antibody (BD Pharmingen, catalog 559257). Cell surface staining was executed with PBS supplemented with 5% FBS and antibodies at 1/100. Cells were incubated for 20 minutes at 4°C. Antibodies used were anti–CD2-FITC (BioLegend, catalog 309205), anti–CD3-PB (BioLegend, catalog 300329), anti–CD4-FITC (Miltenyi Biotec, catalog 130080501), anti–CD5-PECy7 (eBioscience, catalog 25-005942), anti–CD7-FITC (BioLegend, catalog 343103), anti–CD8a-PB (BioLegend, catalog 300927), anti–CD30-APC (Miltenyi Biotec, catalog 130098614), anti–TCRαβ-APC (BioLegend, catalog 306717), and anti–CD45-BV421 (BD Horizon, catalog 563879). NPM-ALK detection was performed with anti–NPM/ALK-PE antibody (BD Pharmingen, catalog 559257). MACSQuant 10 system (Miltenyi Biotec) was used for flow cytometry; data analysis was performed using FlowJo software (BD Biosciences).

Xenograft tumor assay. Mice were housed under pathogen-free conditions in an animal room at constant temperature (20°C–22°C), with a 12-hour light/dark cycle and free access to food and water. Forty-two days after transduction, a total of 3×10^6 CD4$^+$/NPM-ALK$^+$ cells were injected subcutaneously into both flanks (or one flank) or into the tail veins of 5-week-old female NOD/SCID Gamma (NSG) mice (Janvier Labs). Mice received crizotinib (30 mg/kg) or H_2O orally and were treated 5 times per week (Monday through Friday). Mouse body weight and tumor volumes were measured 3 times a week with calipers, using the following formula: length × width^2 × π / 6. At the end of the experiment, mice (6 per group) were humanely sacrificed. Subcutaneous tumors or organs were then excised and sections were fixed in 10% neutral buffered formalin and embedded in paraffin for staining with H&E.

Statistics. Results are presented as mean values ± SEM from at least 3 independent experiments unless otherwise indicated. Differences between groups were examined using the unpaired 2-tailed Student's *t* test, unpaired 2-tailed Student's *t* test with Welch's correction, or 1- or 2-way ANOVA with Bonferroni's posttest, using GraphPad Prism software version 6.00 for Windows (GraphPad software). For all tests, *P* values of less than 0.05 (*), 0.01 (**), or 0.001 (***) were considered statistically significant.

Study approval. We conducted the study in accordance with the Declaration of Helsinki, and approval was received from the relevant CHU Toulouse ethical committees. All animal procedures were performed following the principle guidelines of the INSERM, and our protocol was approved by the Midi-Pyrénées ethic committees on animal experimentation.

Author contributions

FM and CHA designed the research study. CHA, A Congras, NC, and FM performed the experiments. LL was involved in the diagnosis of ALCL. FM and MT performed bioinformatic analysis. PV and A Cieslak performed human thymic subpopulation cell sorting. VA, EM, PB, and GE helped with discussions and critical reading. LR performed human CD34$^+$ CD38^{lo} subpopulation cell sorting. CHA, A Congras, NC, and FM analyzed data. FM wrote the paper.

Acknowledgments

This work was supported by grants from the Ligue contre le Cancer (EL2017.LNCC/PiB to FM), Fondation ARC (PJA20161204769 to FM) pour la Recherche sur le Cancer, and Emergence cancéropole GSO (2016-E14) (to FM); INCa (Projet PAIR Lymphomes) (to LL); and the Labex TOUCAN/Laboratoire d'excellence Toulouse Cancer (to FM, CHA, and A Congras). The authors thank C. Valle and E. Sarot (Pôle Technologique du CRCT – Plateau Genomique et Transcriptomique INSERM-UMR1037) and the staff of the zootechnie Langlade (INSERM/UPS-US006/CREFRE) for technical assis-

tance. The authors extend their warmest gratitude to F. Pflumio, P. Brunet-de-la Grange, J. Calvo, and J. Torrisani for their helpful cooperation. English proofreading was performed by Greenland scientific proofreading. We are grateful to our health care professionals for their boundless investment during the COVID-19 crisis.

Address correspondence to: Fabienne Meggetto, UMR1037 INSERM/Université Toulouse III- Paul Sabatier, ERL5294 CNRS, 2 Avenue Hubert Curien, Oncopole Toulouse, Entrée C, CS 53717, 31037 Toulouse CEDEX 1, France. Phone: 33.5.62.74.45.39; Email: fabienne.meggetto@inserm.fr.

1. Montes-Mojarro IA, Steinhilber J, Bonzheim I, Quintanilla-Martinez L, Fend F. The pathological spectrum of systemic anaplastic large cell lymphoma (ALCL). *Cancers (Basel)*. 2018;10(4):E107.
2. Bonzheim I, Steinhilber J, Fend F, Lamant L, Quintanilla-Martinez L. ALK-positive anaplastic large cell lymphoma: an evolving story. *Front Biosci (Schol Ed)*. 2015;7:248–259.
3. Turner SD, Lamant L, Kenner L, Brugieres L. Anaplastic large cell lymphoma in paediatric and young adult patients. *Br J Haematol*. 2016;173(4):560–572.
4. Lamant L, et al. Prognostic impact of morphologic and phenotypic features of childhood ALK-positive anaplastic large-cell lymphoma: results of the ALCL99 study. *J Clin Oncol*. 2011;29(35):4669–4676.
5. Bisig B, et al. CD30-positive peripheral T-cell lymphomas share molecular and phenotypic features. *Haematologica*. 2013;98(8):1250–1258.
6. Malcolm TI, et al. Anaplastic large cell lymphoma arises in thymocytes and requires transient TCR expression for thymic egress. *Nat Commun*. 2016;7:10087.
7. Ambrogio C, et al. NPM-ALK oncogenic tyrosine kinase controls T-cell identity by transcriptional regulation and epigenetic silencing in lymphoma cells. *Cancer Res*. 2009;69(22):8611–8619.
8. Hoareau-Aveilla C, Meggetto F. Crosstalk between microRNA and DNA methylation offers potential biomarkers and targeted therapies in ALK-positive lymphomas. *Cancers (Basel)*. 2017;9(8):E100.
9. Berdasco M, Esteller M. DNA methylation in stem cell renewal and multipotency. *Stem Cell Res Ther*. 2011;2(5):42.
10. Hassler MR, et al. Insights into the pathogenesis of anaplastic large-cell lymphoma through genome-wide DNA methylation profiling. *Cell Rep*. 2016;17(2):596–608.
11. Moti N, et al. Anaplastic large cell lymphoma-propagating cells are detectable by side population analysis and possess an expression profile reflective of a primitive origin. *Oncogene*. 2015;34(14):1843–1852.
12. Kitagawa Y, Wing JB, Sakaguchi S. Transcriptional and epigenetic control of regulatory T cell development. *Prog Mol Biol Transl Sci*. 2015;136:1–33.
13. Luo CT, Li MO. Transcriptional control of regulatory T cell development and function. *Trends Immunol*. 2013;34(11):531–539.
14. Martinengo C, et al. ALK-dependent control of hypoxia-inducible factors mediates tumor growth and metastasis. *Cancer Res*. 2014;74(21):6094–6106.
15. Zhang Q, et al. The potent oncogene NPM-ALK mediates malignant transformation of normal human CD4(+) T lymphocytes. *Am J Pathol*. 2013;183(6):1971–1980.
16. Christensen JG, et al. Cytoreductive antitumor activity of PF-2341066, a novel inhibitor of anaplastic lymphoma kinase and c-Met, in experimental models of anaplastic large-cell lymphoma. *Mol Cancer Ther*. 2007;6(12 Pt 1):3314–3322.
17. Giuriato S, et al. Conditional TPM3-ALK and NPM-ALK transgenic mice develop reversible ALK-positive early B-cell lymphoma/leukemia. *Blood*. 2010;115(20):4061–4070.
18. Hamedani FS, Cinar M, Mo Z, Cervania MA, Amin HM, Alkan S. Crizotinib (PF-2341066) induces apoptosis due to downregulation of pSTAT3 and BCL-2 family proteins in NPM-ALK(+) anaplastic large cell lymphoma. *Leuk Res*. 2014;38(4):503–508.
19. Mitou G, et al. Targeting autophagy enhances the anti-tumoral action of crizotinib in ALK-positive anaplastic large cell lymphoma. *Oncotarget*. 2015;6(30):30149–30164.
20. Field AE, Robertson NA, Wang T, Havas A, Ideker T, Adams PD. DNA methylation clocks in aging: categories, causes, and consequences. *Mol Cell*. 2018;71(6):882–895.
21. Horvath S. DNA methylation age of human tissues and cell types. *Genome Biol*. 2013;14(10):R115.
22. Egger G, Turner SD. New avenues for targeted therapies and biomarkers in anaplastic large cell lymphoma. *Epigenomics*. 2017;9(2):97–100.
23. Ziller MJ, et al. Charting a dynamic DNA methylation landscape of the human genome. *Nature*. 2013;500(7463):477–481.
24. Lamant L, et al. Gene-expression profiling of systemic anaplastic large-cell lymphoma reveals differences based on ALK status and two distinct morphologic ALK+ subtypes. *Blood*. 2007;109(5):2156–2164.
25. Jung N, Dai B, Gentles AJ, Majeti R, Feinberg AP. An LSC epigenetic signature is largely mutation independent and implicates the HOXA cluster in AML pathogenesis. *Nat Commun*. 2015;6:8489.
26. Koues OI, et al. Distinct gene regulatory pathways for human innate versus adaptive lymphoid cells. *Cell*. 2016;165(5):1134–1146.
27. Schleussner N, et al. The AP-1-BATF and -BATF3 module is essential for growth, survival and TH17/ILC3 skewing of anaplastic large cell lymphoma. *Leukemia*. 2018;32(9):1994–2007.
28. Bhatt RS, et al. Hypoxia-inducible factor-2alpha: effect on radiation sensitivity and differential regulation by an mTOR inhibitor. *BJU Int*. 2008;102(3):358–363.
29. Covello KL, et al. HIF-2alpha regulates Oct-4: effects of hypoxia on stem cell function, embryonic development, and tumor growth. *Genes Dev*. 2006;20(5):557–570.
30. Petruzzelli R, Christensen DR, Parry KL, Sanchez-Elsner T, Houghton FD. HIF-2α regulates NANOG expression in human embryonic stem cells following hypoxia and reoxygenation through the interaction with an Oct-Sox cis regulatory element. *PLoS One*. 2014;9(10):e108309.
31. Ellis TM, Simms PE, Slivnick DJ, Jack HM, Fisher RI. CD30 is a signal-transducing molecule that defines a subset of human activated CD45RO+ T cells. *J Immunol*. 1993;151(5):2380–2389.
32. van der Weyden CA, Pileri SA, Feldman AL, Whisstock J, Prince HM. Understanding CD30 biology and therapeutic targeting: a historical perspective providing insight into future directions. *Blood Cancer J*. 2017;7(9):e603.
33. Montel-Hagen A, et al. Organoid-induced differentiation of conventional T cells from human pluripotent stem cells. *Cell Stem Cell*. 2019;24(3):376–389.
34. Seet CS, et al. Generation of mature T cells from human hematopoietic stem and progenitor cells in artificial thymic organoids. *Nat Methods*. 2017;14(5):521–530.
35. Laurent C, et al. Circulating t(2;5)-positive cells can be detected in cord blood of healthy newborns. *Leukemia*. 2012;26(1):188–190.
36. Maes B, et al. The NPM-ALK and the ATIC-ALK fusion genes can be detected in non-neoplastic cells. *Am J Pathol*. 2001;158(6):2185–2193.
37. Trumper L, Pfreundschuh M, Bonin FV, Daus H. Detection of the t(2;5)-associated NPM/ALK fusion cDNA in peripheral blood cells of healthy individuals. *Br J Haematol*. 1998;103(4):1138–1144.
38. Forristal CE, Wright KL, Hanley NA, Oreffo RO, Houghton FD. Hypoxia inducible factors regulate pluripotency and proliferation in human embryonic stem cells cultured at reduced oxygen tensions. *Reproduction*. 2010;139(1):85–97.
39. Rouault-Pierre K, et al. HIF-2α protects human hematopoietic stem/progenitors and acute myeloid leukemic cells from apoptosis induced by endoplasmic reticulum stress. *Cell Stem Cell*. 2013;13(5):549–563.
40. Lamant L, et al. Establishment of a novel anaplastic large-cell lymphoma-cell line (COST) from a 'small-cell variant' of ALCL. *Leukemia*. 2004;18(10):1693–1698.
41. Congras A, et al. Doxorubicin-induced loss of DNA topoisomerase II and DNMT1- dependent suppression of MiR-125b induces chemoresistance in ALK-positive cells. *Oncotarget*. 2018;9(18):14539–14551.
42. Love MI, Huber W, Anders S. Moderated estimation of fold change and dispersion for RNA-seq data with DESeq2. *Genome Biol*. 2014;15(12):550.
43. Huber W, et al. Orchestrating high-throughput genomic analysis with Bioconductor. *Nat Methods*. 2015;12(2):115–121.